# Multi-platform LiDAR approach for detecting coarse woody debris in a landscape with varied ground cover

Shukhrat Shokirov[1,2], Michael Schaefer[3], Shaun R. Levick[2], Tommaso Jucker[4], Justin Borevitz[1], Ilhom Abdurahmanov[5], Kara Youngentob[1]

[1]*Research School of Biology, Australian National University, Australia*

[2]*Commonwealth Scientific and Industrial Research Organization, Land and Water, Australia*

[3]*Food Agility CRC Ltd, 81 Broadway, Ultimo, NSW, 2007, Australia*

[4]*School of Biological Sciences, University of Bristol, England*

[5]*Tashkent Institute of Irrigation and Agricultural Mechanization Engineers, Uzbekistan*

## Abstract

Coarse woody debris (CWD), or fallen logs, are known to be an essential habitat element for many organisms. CWD also supports ecosystem functioning through soil formation, nutrient cycling, and carbon storage. For these reasons, accurate assessments of CWD across landscapes are of interest to many ecologists and landscape managers, but traditional field-based measurements can be time-consuming and sampling strategies may not be representative of entire landscapes. Light detection and ranging (LiDAR) technologies may be able to provide a more rapid assessment of the number and volume of CWD across wide-areas. However, most research using LiDAR for forest and woodland inventory assessment has focused on standing wood. Detection accuracy of CWD with LiDAR can be impacted by the point density of LiDAR data, ground layer vegetation and sensor positioning relative to other vegetation or landscape structural features. We used high resolution terrestrial laser scanner (TLS), unoccupied aerial vehicle (UAV) laser scanner (ULS) and a combination of data from both sensors (i.e., fused data, FLS) to estimate CWD in a grassy woodland ecosystem. The study area comprised plots with different types and amounts of vegetation cover and different types of CWD, both naturally occurring and introduced including dispersed, clumped or a mixture of both types. This enabled a more detailed exploration of model performance across sensor types, vegetation types and ground cover biomass. A random forest (RF) classification algorithm and noise removing operations on raster imagery were used to classify CWD. Completeness and correctness accuracy with the developed method were highly variable depending on the data and ground vegetation cover, and ranged between 20% and 86%, and 12% and 96%, respectively in comparison with field data. LiDAR derived digital surface model (DSM), surface roughness and topographic position index were important variables for CWD detection. We found that the detection accuracy of CWD varied with the vegetation type, amount of ground vegetation cover and LiDAR data. Ground cover density had a strong negative impact on accuracy, particularly for TLS and FLS data.

**Keywords:** TLS, UAV laser scanning, LiDAR, Coarse Woody Debris, Random Forest, habitat

## 1. Introduction

Coarse Woody Debris (CWD), or fallen dead trees, are an important structural component in forest ecosystems that provide habitat for plants and animals. CWD provides shelter, nesting areas and a foraging substrate for many bird, reptile and mammal species (Harmon et al. 2004; Manning et al. 2013). CWD also has a role in multiple aspects of ecosystem functioning including soil formation, nutrient cycling, and carbon storage (Harmon et al. 2004; Woldendorp and Keenan 2005; Manning et al. 2013). CWD is a naturally occurring feature of forests and woodlands, but it is often removed for firewood or lost through land-clearing or other landscape management practices (e.g., post-logging burning of forests) (West et al. 2008; Manning et al. 2013).

The loss of CWD from an ecosystem causes a reduction or loss of the associated biodiversity and ecological processes over short and long time periods (Manning et al. 2013). The natural accumulation rate of CWD is usually very slow and depends on a number of factors including tree genetics, stand age and anthropogenic or natural disturbance (Vandekerkhove et al. 2009). Restoring CWD is an increasingly common intervention to support biodiversity conservation and improve other ecosystem services such as carbon storage and soil improvement (Manning et al. 2004).

Measuring the amount, volume, diameter and length of CWD is important for monitoring this resource and estimating habitat quality for a number of CWD dependent organisms (Harmon et al. 2004). Traditional field-based methods of CWD data collection are usually restricted to transects and plots, which are time-consuming and may not accurately represent the entire area from which the subsample is taken (Harmon et al. 2004; Lopes Queiroz et al. 2020). Thus, remote sensing may be a valuable tool to overcome these drawbacks and quantify CWD across wide-areas. A few studies have attempted to classify and quantify CWD using aerial multispectral imagery (Smikrud and Prakash 2013; Windrim et al. 2019). However, shading and canopy occlusion interfere with the ability of multispectral imagery to map CWD in many environments (Blanchard et al. 2011; Richardson and Moskal 2016).

The rapidly developing technology of Light Detection and Ranging (LiDAR) offers an alternative remote sensing technique for mapping CWD by capturing three-dimensional landscape structure and vegetation (Pasher and King 2009; Marchi et al. 2018). LiDAR can be used from airborne or terrestrial platforms and the combined data from both platforms may help address occlusion issues unique to the perspective of airborne or terrestrial sensors. LiDAR uses a laser light to measure the distance between the sensor and ground features. A single pulse emitted from a LiDAR sensor can capture structural information from different layers of vegetation, including upper canopy, lower canopy and other elements near the ground (Lefsky et al. 2002; Bergen et al. 2009).

Relatively few studies have used LiDAR to quantify CWD, since most LiDAR-based measurements of forest and woodland structure have focused on standing wood. However, as this technology becomes more accessible, ecologists are increasingly interested in using

LiDAR technology for investigating important below canopy structural habitat features such as CWD (Pesonen et al. 2009; Lopes Queiroz et al. 2020). A small number of studies have identified some LiDAR based metrics that may be useful for mapping CWD. For example, Pesonen et al. (2009) predicted CWD volume from airborne laser scanning (ALS) derived canopy height percentiles using regression analysis, and Mücke et al. (2013) utilized surface roughness features derived from full-waveform and discrete return ALS data to classify CWD. In addition, Object Based Image Analysis (OBIA) has been successfully applied using Trimble eCognition software to ALS derived raster images for automatically delineating CWD in disturbed open forest (Blanchard et al. 2011). Lopes Queiroz et al. (2019; 2020) performed geographic object based image analysis (GOBIA) with a random forest (RF) classifier in eCognition commercial software using a ALS derived digital surface model, canopy height model and aerial multispectral imagery to classify CWD. Their research is the first and only previous study that used RF models with combined ALS and multispectral imagery to detect CWD. Notably, data from unoccupied aerial vehicle laser scanning (ULS) has not been used in any prior assessments of CWD.

LiDAR-derived raster images are more often used for automatically classifying CWD (Marchi et al. 2018), but a few studies have attempted to extract CWD from high density terrestrial laser scanning (TLS) point cloud data (Polewski et al. 2017; Yrttimaa et al. 2019). For instance, Polewski et al. (2017) used a statistical framework to fit a cylinder shape over a TLS data to detect CWD. Yrttimaa et al. (2019) also used a cylinder fitting algorithm on TLS point cloud data followed by raster image filtering to quantify the number and volume of CWD. Despite some successes, accurate detection of CWD below the canopy using LiDAR technology remains a challenging task and depends largely on the point density of LiDAR point cloud and surrounding vegetation height and density (Polewski et al. 2017).

All of the above-mentioned studies found a negative impact of ground vegetation cover on CWD detection accuracy; however, most were conducted in optimal low groundcover conditions with a single sensor type, so it was not possible to compare model performance across different amounts of vegetation cover or with data collected from different sensors or platforms. For the first time, we look at the effects of ground vegetation cover on model performance using UAV (unoccupied aerial vehicle) laser scanning (ULS), terrestrial laser scanning (TLS), and a combination of data from both sensors (i.e., fusion, FLS). We utilized surface topographic variables derived solely from high resolution LiDAR datasets as inputs into RF in open source R language (R Core Team 2020) to test a novel approach to classify and quantify CWD.

The aim of this study was twofold:

1) To investigate the performance of Random Forest (RF) machine learning algorithms to quantify CWD from commonly used LiDAR derived topographic surface variables.
2) To test the influence of vegetation type and ground cover on CWD assessment accuracy using ULS, TLS and FLS datasets.

## 2. Materials and methods

### 2.1. *Study Area*

This study was conducted in Mulligan's Flat (683 ha) and Goorooyarroo (702 ha) (MFGO) nature reserves, located in the north-eastern corner of the Australian Capital Territory (ACT), (35°09' S-149°09' E; Fig. 1). Elevation ranged between 650-700 meters with a gently undulating topography that includes low rolling hills interspersed with plains and flats (McIntyre et al. 2010). These two adjacent wildlife reserves were established in 1994 and 2006, respectively, to conserve and restore a critically endangered yellow box–Blakely's red gum grassy woodland ecosystem (Manning et al. 2011). Restoration activities include, but are not limited to, the introduction of CWD, pest exclusion fences and the reintroduction of previously locally extinct native species (Manning et al. 2013).

As part of on-going experimental restoration work at MFGO, 96×1 ha (200 m × 50 m) sites were established across both reserves in 24 clusters and include four different vegetation types: 1) high tree, high shrub cover (HTHS), 2) high tree, low shrub cover (HTLS), 3) low tree, low shrub cover (LTLS), and 4) low tree, high shrub cover (LTHS) (Manning et al. 2011) (Fig.1). In October 2007, two-thousand tonnes of CWD were distributed across 72 sites in both reserves. The remaining sites with no introduced CWD served as controls. Treatments were: (a) 20 tonnes/ha added with dispersed CWD, (b) 20 tonnes/ha added with clumped CWD, and (c) 40 tonnes/ha added with both dispersed and clumped CWD (Manning et al. 2007) (Figs. 1 and 2). Detailed information on the addition of CWD is provided in (Manning et al. 2013).

[Figure 1 Here]

[Figure 2 Here]

### 2.1. *TLS data collection and post - processing*

We collected TLS data with a high-density terrestrial laser scanner (Topcon GLS2000, Topcon Corporation, Japan) that emits near-infrared light (1064 nm) laser pulses at up to 120,000 laser pulses per second. The field-of-view of the scanner is 360° horizontally and 270° vertically. A single laser pulse has a beam diameter of 4 mm at 60 m. Data was collected from 7 scan stations in each 50 m × 200 m plot in a zigzag formation with approximately equal spacing (33 m) between the stations. The number and arrangement of scan stations was determined by a pilot study to identify the optimal number and arrangement of scans to characterise all 96 sites within a one month timeframe (Shokirov et al. 2020; Shokirov 2021). From the 1$^{st}$ to 31$^{st}$ of October 2018, TLS LiDAR data was acquired across all 96 × 1 ha sites for a total of 672 scans with 6 mm at 10 m scanning resolution and 1.7 m scanning height. The position of each scan was measured with a differential GPS (Trimble Geoexplorer 6000 series) and post-processing was performed using local base station data to improve the location accuracy to approximately 0.5 m.

Point clouds from the seven individual scan stations for each plot were co-registered using the Multi-station Adjustment (MSA) plugin in RiScan Pro software (RIEGL Laser Measurement Systems GmbH). Co-registering point clouds with MSA consists of two steps: manual and automatic registration. First, point clouds from two scans were manually coarsely aligned by using the overlapping objects (trunks, trees and shrubs) in both scans. Then, automatic registration was implemented, which uses at least four identical points from overlapping areas of two scans. MSA uses the iterative closest points (ICP) algorithm that minimises the 3D distance between the identical points by translating and rotating the entire point cloud along x, y, z axes until the least minimum distance between the identical points from two dataset is achieved (Šašak et al. 2019). Then the position and orientation of the first and second scan were locked and the same procedure was performed to register the third scan to the initial two scans.

Next, the point cloud from each site was georeferenced using DGPS locations of each scan position measured in the field and clipped to the spatial extent of the 96 sites individually. Point clouds were then subsampled into 1 cm spacing to homogenize the point distributions and duplicate points were removed using CloudCompare software (CloudCompare 2020).

### *2.3. ULS data collection and post-processing*

We obtained ULS data across all of the 96 sites in fine weather conditions from the 7th until the 14th of November, 2018. The ULS LiDAR platform consisted of a hexacopter integrated with a RIEGL miniVUX-1 UAV LiDAR sensor (RIEGL Laser Measurement Systems GmbH, Austria) and an APX-15 INS/GNSS system (Trimble, USA). ULS data was acquired at approximately 80 m above the take off point at approximately 7 m $s^{-1}$, with up to 5 returns per pulse, 100 kHz pulse repetition rate, and up to 100,000 measurements/second. The maximum scan angle of the LiDAR sensor was approximately ±60º with swath width of approximately 100 m. On average, the four adjacent plots were covered by 500 × 500m flight area which included 11 parallel lines and one diagonal flight line on the return to landing. We used DJI ground station pro V2 to plan the flight missions (SZ DJI TECHNOLOGY CO. 2018). The ULS LiDAR sensor failed to collect data on two 1 ha sites, which were excluded from further analysis of ULS and TLS data. Data processing was done in RiPROCESS software suite from RIEGL to bring in the trajectory data of the drone flight, align the flight paths, geo-reference the point cloud and then export it in ASPRS LAS format. The trajectory data of the UAV LiDAR that was ingested into RiPROCESS was generated using POSPAC UAV (Applanix) using the IMU/GNSS data from the drone and RINEX data from the base station, which was obtained from the Gungahlin location of Smartnet global network.

The ULS LiDAR data collected over the 94 sites were clipped by corresponding polygons to create separate point clouds for each site. In general, point spacing in ULS data across 94 sites ranged from 5 cm to 17 cm with an average of 10 cm. For this reason, we homogenized the point cloud with 10 cm spacing and removed duplicate points using CloudCompare software (CloudCompare 2020).

### *2.4. Field data*

Field data collection for ground-truthing the model outputs was conducted in June, 2020. Eighteen sites were selected that included the three CWD types and four different vegetation types across both reserves. CWD in our research is defined as the downed dead wood including tree trunks and branches at least 2 m in length and 0.1 m in diameter. The minimum diameter of 0.1 m was determined based on the point spacing of ULS data (approximately 0.1 m), which indicated that ULS should be able to capture CWD with at least 0.1 m diameter and this aligned with the minimum size identified in other studies as well (Pesonen et al. 2009; Farnell et al. 2020). The length of 2 m is commonly used for defining of CWD for forest inventory (Grizzel et al. 2000; Edwards 2004). The location of the centre of each individual log was recorded with a differential GPS (± 3 m accuracy). For clumped logs, a single location at the nearest midpoint of the clump was measured. Photos of each clumped and dispersed CWD were also taken.

The volume of each CWD was calculated using the cylinder volume equation:

$$V_{field} = l \times \pi \times ({}^{d}/_{2})^2 \quad \text{Equation (1)}$$

Where, $V_{field}$ - volume of CWD, $l$ - length of CWD, $d$ - diameter in the middle of the full length of CWD, $\pi$ - mathematical constant.

To estimate the influence of ground cover on CWD detection accuracy, sample sites were divided into three different ground cover categories: Low (< 400 kg/ha), Medium (400 kg/ha - 800 kg/ha) and High (> 800 kg/ha) (Fig. 2). This classification was based on an earlier study (McIntyre et al. 2010), which estimated total biomass (kg/ha) of native and exotic plants across the 96 sites at MFGO. Although this previous study was conducted in 2010, the differences in ground vegetation cover were primarily driven by vegetation species and herbivore exclusion fencing at a subset of sites, which have not changed substantially over this period, and this was confirmed through a visual comparison of sites to their earlier classification by McIntyre et al. (2010).

### *2.5. Merging the TLS and ULS data*

A fused dataset (FLS) was created from TLS and ULS data first by manually adjusting and then automatically co-registering the data from both sensors using the Iterative Closest Point (ICP) algorithm in CloudCompare (CloudCompare 2020).

### *2.6. Noise reduction, normalization and subsetting the point clouds*

TLS, ULS and FLS point clouds were cleaned for noise with *lasnoise* with step 0.30 (TLS and FLS) and step 0.50 (ULS) parameters. Point clouds were classified into ground and non-ground points using the *lasground* tool in LAStools (Isenburg 2012). *Lasground* uses progressive, Triangulated Irregular Network (TIN) densification methods to classify ground points (Montealegre et al. 2015). Different settings of *lasground* were trialed and the resulting ground and non-ground points were visually assessed across different plots. This was important because improper filtering of ground points might result in incomplete or false CWD surface points. The final selected *lasground* setting were as follows: *step 2, extra_fine, not_airborne, compute_height, replace_z* for TLS and FLS dataset and the same parameters except without *not_airborne* for ULS dataset (Isenburg 2012). Using field measurements, it was found that the height of almost all of the CWD was less than 1 m. Thus, a subset of point clouds of all 94 sites was created by removing the points above 1.3 m to provide an additional height buffer.

### *2.7. CWD extraction workflow*

#### *2.7.1. Calculating DSM and other topographic variables*

CWD classification involved machine learning methods with imagery data. First a 0.1 m grid-size digital surface model (DSM) was created from all returns below 1.3 m using *las2dem* (Isenburg 2012) for all three datasets (TLS, ULS and FLS). The *las2dem* module of LAStools first creates a Triangulated Irregular Networks (TIN) and then generates an interpolated raster image from TIN (Khosravipour et al. 2014; Stereńczak et al. 2016). After testing several parameters, “elevation” and “step 0.1” were chosen to create the DSM. In addition, a parameter of “kill 0.25” was used to avoid creating the DSM from triangles with edge longer than 0.25m. This was done to avoid creating false planar objects in occluded areas in the plot that might have caused false positives in the RF model. To reduce the noise and generate a smoothed DSM, a Gaussian Filter algorithm in SAGA (Conrad et al. 2015) was used with the following parameters (standard deviation: 1, search mode: square, search radius: 3). Subsequently, DSMs from all dataset were imported to RStudio environment and five topographical variables were calculated to characterize the shape of relief from DSM using a raster package (Hijmans 2020). An 8×8 moving window on the underlying DSM layer was used to compute slope and aspect variables. All six variables were stacked together to create a six band raster image. Previous studies have found these variables useful for characterizing the spatial heterogeneity of landscape surfaces (Amatulli et al. 2018). The list of variables and their descriptions are shown in Table 1. In addition, the relationship between the topographic variables derived from TLS, ULS and FLS datasets were examined using Pearson’s correlation (Appendix 1).

[Table 1 Here]

### *2.7.2. Training data preparation*

To create a training dataset, CWD, shrub and grass classes were delineated based on the visual assessment of DSM and its shaded relief data using QGIS software (QGIS.org 2021). Training samples distributed across the landscape from each class (CWD, shrub, and grass) were collected from most of the 94 sites to avoid spatial autocorrelation in the training dataset (Millard and Richardson 2015). To avoid imbalanced data, which can negatively impact classification accuracy (Maxwell et al. 2018), approximately 300 samples per class were collected. A distance of at least 8 m between the classes was kept to avoid spatial interpolation, as recommended (Millard and Richardson 2015).

### *2.7.3. Random forest classification*

Random Forest (RF) is a widely used machine learning technique for classifying remote sensing data (Guo et al. 2011; Millard and Richardson 2015). Many studies found that machine learning algorithms produce higher accuracy remote sensing classifications than traditional pixel based algorithms like maximum likelihood (Duro et al. 2012; Maxwell et al. 2018).

We ran RF classifications using the ‘caret’ package (Kuhn 2020) in R statistical software (R Core Team 2020). The caret package provides a standard syntax to execute a variety of machine-learning methods (Maxwell et al. 2018). The RF is a tree-type classification algorithm which utilizes a set of decision trees to make a prediction (Breiman 2001; Belgiu and Drăguţ 2016). First, training data are created by delineating small subsets of polygons as a sample of target classes on an image. Then, the algorithm trains the data by generating multiple decision trees where each tree is trained based on randomly sampling the variables in the original training data set (Belgiu and Drăguţ 2016). Each decision tree will come up with a rule to predict a target class. Each tree produces a vote to a target class and these votes will be counted and the majority vote of trees will be used for classification (Breiman 2001; Friedman et al. 2001).

Two parameters of the RF model can be tuned by the user: the number of decision trees ($T$) and the number of variables ($M$) randomly chosen at each split. However, multiple studies have found that tuning the number of $T$ manually does not impact the accuracy of the results as long as the number of $T$ is large enough (>300) (Probst and Boulesteix 2017; Maxwell et al. 2018). Therefore, we selected a conservative number of 500 $T$ in the caret package (Maxwell et al. 2018). The default setting of three randomly chosen variables $M$ was kept at each split.

A previous study found that highly correlated predictor variables reduced the classification accuracy (Millard and Richardson 2015). Hence, Pearson’s correlation was used to calculate pair-wise correlations between the predictor variables, and variables that were highly correlated ($r > 0.9$) to any other predictor variable were removed (Millard and Richardson 2015). To test model performance, training samples were split into training and testing datasets using proportional stratified random sampling. Approximately 70% of the samples were used to train the data using the RF algorithm and the remaining 30% of the data were reserved as a "hold-out" to test the classification accuracy (Duro et al. 2012). Model performance was examined with out-of-bag error (OOB) and confusion matrixes to estimate classification accuracy between predicted and observed data in the hold-out 30% independent validation data (Millard and Richardson 2015). We also evaluated the importance of predictor variables for the classification accuracy using OOB.

#### *2.7.4. Post-classification refinement and shape analysis*

Remote sensing data classification often requires post-classification improvement to reduce noise from classification maps (Droppova 2011; Boz et al. 2015). We used the Majority Filter tool in ArcMAP (ESRI 2011) for smoothing the image. Majority filter replaces cells in a raster based on the majority of their contiguous neighboring cells, and as a result, most of the isolated pixels will be assigned to a surrounding class. Then, only CWD class pixels were converted to polygon shapefiles using the Raster to Polygon conversion tool in ArcMAP (ESRI 2011). After the polygon smoothing algorithm, polygons with areas greater than 0.2 $m^2$ and less than 25 $m^2$ were selected. These thresholds were derived from the minimum area of CWD (0.1 m width and 2 m length) and visual interpretation of DSM and polygons, respectively. Elongated objects were extracted by creating a minimum bounding box for each polygon and the width and length of each box was calculated. Then, bounding boxes with lengths of less than 2 m were removed. Finally, polygons within remaining bounding boxes were selected using Select by Location tool in ArcMAP (ESRI 2011).

### *2.7.5. Calculating volume of CWD*

A Zonal Statistics tool in QGIS software (QGIS.org 2021) was used to calculate a volume for each detected CWD. This tool calculates several values including mean value of all pixels, number of all pixels and sum of pixels from DSM for each overlapping polygon. Volume of CWD was derived from the following equation:

$V_{detect} = A^2 \times M \times C$ Equation (2)

Where, $V_{detect}$ − volume, $A$ − pixel size, $M$ − mean value of all pixels within a polygon, $C$ − number of pixels within a polygon.

Consequently, total CWD volume for each site was calculated using the sum of all CWD volume in the site.

### *2.7.6. Classification accuracy assessment*

Classification accuracy was performed by comparing the CWD vector map and field-measured coordinates of each CWD in the 18 validation sites. DSM, DSM-based shaded relief and photos from the field were also used to assist with accuracy assessments. For each of the 18 sample sites, Producer’s accuracy (completeness) and User’s accuracy (correctness) were estimated using Equations 3 and 4, respectively (Mücke et al. 2013). To evaluate the accuracy of estimated CWD volume, field data of CWD volume from each plot and detected CWD volume (excluding FP), and detected total CWD volume (including FP) were compared. We excluded FP to determine the accuracy of CWD volume estimates where CWD is correctly detected. To assess the impact of FP in estimated CWD volume, we then included both TP and FP in the accuracy assessment.

$Completeness = TP/(TP + FN)$ Equation (3)

$Correctness = TP/(TP + FP)$ Equation (4)

Where, a True Positive (TP) is a CWD that is detected by the method and is recorded in the field data, a False Positive (FP) is a CWD that is detected but is not recorded in the field data, and a False Negative (FN) is a CWD that is not detected but is present in the field data.

The difference between the detected and ground measured CWD volume were estimated using the coefficient of determination ($R^2$) and the Root Mean Square Error (RMSE, Equation 5). The CWD detection workflow is provided in Figure 3.

$$RMSE = \sqrt{[\frac{\sum(P_i - O_i)^2}{n}]} \quad \text{Equation (5)}$$

Where, $\Sigma$ symbol indicates "sum", $P_i$ is the predicted volume for the $i$ th observation, $O_i$ is the observed volume for the $i$ th observation, $n$ is the sample size.

[Figure 3 Here]

# 3. Results

## *3.1. CWD field data*

We measured a total of 998 CWDs from 18 sites for ground-truthing. The average amount of CWD in a site was 55, the max amount was 93 and the min amount was 33. Sites with dispersed and clumped CWD had the same number on average (n = 47 and n = 46, respectively), but combined (clumped and dispersed in the same site) had a substantially higher number of CWD on average (n = 71). The length of CWD ranged from 2 m to 14 m (mean of 4.1m), and diameter in the middle of the long axis ranged from 0.1 m to 0.9 m (mean of 0.3 m). The volume of a single CWD varied from 0.02 $m^3$ to 3.98 $m^3$ (mean value of 0.37 $m^3$) (Appendix 2).

## *3.2. Variable selection and comparison across TLS, ULS and FLS data types*

Pearson's pair-wise correlations between the predictor variables indicated that surface terrain ruggedness index and slope correlated highly with other variables ($r$ > 0.9) (Appendix 3).

Hence, they were removed and the remaining variables, DSM, Roughness, Topographic Position Index (TPI) and Aspect raster images, were used as predictors in the RF classification.

Pearson's correlation was also used to investigate the relationship between TLS, ULS and FLS derived surface topographic variables (Appendix 1). ULS and FLS typically demonstrated stronger correlation among common variables than ULS and TLS but substantially less than TLS and FLS (Appendix 1). TPI and aspect showed the weakest correlations across the data types. The highest correlation among variables was observed between TLS and FLS, with $r > 0.8$ between the two data types for DSM, slope, TRI and roughness (Appendix 1).

### *3.3 Accuracy assessment of RF model*

RF classification was performed on the aforementioned four predictor variables and training samples. Overall classification accuracy of the independent testing data varied between different sensors with TLS (72.5%), ULS (75.5%) and FLS (78.2%) (Table 2). Confusion matrices, which describe correctly and incorrectly classified pixels of the predicted classes compared to the testing dataset indicated that the model performed best in classifying grass classes (> 80.2%) but had a lower classification accuracy for CWD ( > 67.9%) and shrub classes (> 66.9%) (Table 2).

[Table 2 Here]

The OOB errors produced by RF for an accuracy assessment using the independent (hold-out) testing data as well as measures of variable importance based on the mean decrease in accuracy when a variable is not used in building a tree are presented in Figure 4. OOB error is lowest for the grass class and higher for shrub and CWD classes across different sensor data. Average OOB error is lowest for FLS data (≈22%) and higher for ULS (≈25%) and TLS (≈28%) data. Overall, accuracy assessment by OOB error is consistent with the confusion matrix described in Table 2.

[Figure 4 Here]

In general, DSM and surface roughness were the most important predictor variables in classifying CWD, shrubs and grass (Fig. 5). DSM, roughness and TPI were comparably important for identifying CWD from all three types of data. Surface aspect had the weakest prediction power for classifying all classes (Fig. 5).

[Figure 5 Here]

### *3.3. Accuracy assessment of CWD counts*

#### *3.3.1. Overall accuracy*

Both sensors produced comparable completeness accuracy in counting the number of CWD and exhibited large variations in accuracy between sites (TLS = 19.6% to 75.0%, average of 57.0%, ULS = 32.8% to 82.2%, average of 57.8%) (Table 3). However, correctness accuracy for TLS was slightly higher (11.9% to 96.2%, average of 55.5%) than ULS (29.4% to 81.1% average of 51.7%). FLS data outperformed single sensors in counting CWD for both completeness and correctness accuracy (averages = 67.0% and 55.6%, respectively), indicating that co-registering TLS and ULS sensor data improved the accuracy for this measure (Table 3).

[Table 3 Here]

#### *3.3.2. CWD count accuracy by varied ground cover density*

Ground vegetation cover had the biggest impact on CWD detection accuracy for the TLS sensor (Table 4). We found a roughly similar completeness accuracy across the sites with differing amounts of ground vegetation. However, ground vegetation had a big influence on correctness accuracy for TLS and FLS and to a lesser extent for ULS based counts (Table 4) (Fig. 6).

[Table 4 Here]

[Figure 6 Here]

### *3.3.3. CWD count accuracy by vegetation cover types*

Our method achieved comparable average completeness accuracy from different sensor data across LTHS, HTHS and HTLS vegetation types (Table 5). However, FLS data provided significantly higher average completeness accuracy in plots with the LTLS vegetation type compared to the TLS and ULS data. HTHS vegetation type had a stronger negative impact on the correctness accuracy of CWD counts from TLS and FLS data than ULS data (Table 5).

[Table 5 Here]

### *3.3.4. CWD volume accuracy*

Using only True Positives, predictions of CWD volume was best achieved by ULS ($R^2$ = 0.70, RMSE = 6.9 $m^3$) and FLS data ($R^2$ = 0.67, RMSE = 5.7 $m^3$). Predicted volume from TLS data with only True Positives had a relatively weak correlation with observed volume ($R^2$ = 0.43, RMSE 8.5 $m^3$) (Fig. 9, a). The predicted CWD volume was overestimated across all sensors.

When considering both True Positives and False Positives, there was a weak correlation between predicted and observed CWD volume from all types of data (Fig. 7, $a_1$, $b_1$, $c_1$). The relationship between predictions of CWD volume and field based CWD volume for TLS ($R^2$ = 0.05, p = 0.36) and FLS ($R^2$ = 0.21, p = 0.059) data was not significant at the 95% confidence level. However, ULS data performed better than the other data types in predicting CWD volume with data that included True and False positives ($R^2$ = 0.26, p = 0.032). False Positives had a strong negative effect on calculating CWD volume (Fig. 7, $a_1$, $b_1$, $c_1$).

[Figure 7 Here]

## 4. Discussion

To our knowledge, this is the first study that used data from TLS, ULS and a fusion of both sensors (FLS) to classify CWD across a variety of vegetation types and different amounts of ground vegetation cover. We used a RF machine learning classification algorithm with DSM and DSM-based surface variables to extract CWD from other ground attributes including grass and shrubs. The models performed best for classifying grass cover, followed by CWD and shrubs, with significantly varied results depending on the type of data. Our model indicated that LiDAR derived DSM, surface roughness and TPI variables contributed the most to classifying CWD. The ability to quantify CWD, in number and volume, showed variable success and large differences across sensors and landscape types.

While there are advantages of combining sensor data to obtain more complete coverage, particularly where TLS data has occlusions from ground vegetation and ULS may not be able to completely penetrate the dense canopy vegetation, in situations with high vegetation ground cover, the ULS platform outperformed TLS and FLS data in the open woodland landscape. Against our expectations, FLS data did not improve the model on sites with higher ground cover. However, FLS data from sites with low tree and low shrub (LTLS) cover resulted in the most accurate CWD counts with our methodology.

A recent study classified CWD in a boreal forest using RF classifier with higher accuracy (>90%), but ground vegetation density was lower and the effects of vegetation cover were not assessed (Lopes Queiroz et al. 2019). That study utilized a combination of optical imagery and ALS LiDAR derived DSM and although model performance was good, accuracy assessments were based on cross-validation alone, rather than an independent testing dataset of field measured CWD (Lopes Queiroz et al. 2019). While ALS has shown promise in CWD assessments like these, the ability of ALS imagery to detect CWD smaller than 0.3m diameter is typically poor, due mainly to low point density and beam foot-print size (Marchi et al. 2018).

In addition, although LiDAR can provide a number of surface variables, those studies used only LiDAR based DSM as an input variable (Blanchard et al. 2011; Lopes Queiroz et al. 2019). In this study, we found that, in addition to DSM, other surface variables such as roughness, aspect, topographic position index can contribute to improve CWD classification accuracy.

**Effects of vegetation type and ground cover on model performance**

Many previous studies have mentioned that ground cover can impact the ability of LiDAR sensors to detect and measure CWD (Polewski et al. 2017; Marchi et al. 2018). However, none have attempted to compare the accuracy of LiDAR-based CWD models across different ground cover densities. Our study examined this impact by including sites with high, medium and low ground cover biomass. As expected, high ground cover biomass resulted in more false positives in the classification and counts of CWD, which substantially decreased correctness accuracy and this effect was strongest in the TLS and FLS data compared to ULS data (Table 4). In addition, models from ULS data performed better than TLS or FLS models in sites with the most ground cover biomass, which was demonstrated by a lower number of false positives. The ULS sensor obtained data from above the sites, and this improved the classification of CWD, which may have been obscured by dense vegetation features on the ground when LiDAR data was obtained from a sensor positioned at the ground. For this reason, with the proposed method, TLS sensors may not be appropriate for detecting CWD in a landscape with high ground vegetation cover. Notably, we collected 7 TLS scans in each site, which was the minimum number of scans required to characterize each 200 m × 50 m area (Shokirov 2021). More scans per site in a traditional grid-sampling design would likely improve the TLS performance and the reasons for these are discussed in the next section. Low and medium ground vegetation cover had less influence on completeness and correctness accuracy across all types of sensor data.

The total volume of CWD tended to be overestimated by all the sensors. This may have been a result of the interpolation techniques when creating raster imagery. When considering both true and false positives, only ULS data indicated significant prediction power of CWD volume. TLS sensor data resulted in a particularly high overestimation of site-level CWD volume, due to the high sensitivity of TLS to other ground-based objects. High ground cover sites in the study area contained dense, clumped vegetation species such as *Joycea pallida*, *Austrodanthonia* spp., and *Aristida ramose* (McIntyre et al. 2010) (Fig. 2). These types of grasses tend to create two problems for CWD detection: 1) they block the TLS laser pulses (occlusion error), which limits detection of CWD from distances over 10 m, and 2) the algorithm can have difficulty distinguishing CWD from the clumped vegetation, and consequently creates many false positives. Although fusing TLS with ULS may help overcome the first problem, the latter problem influenced the FLS dataset as it still contains TLS data, which created false positives when the landscape is covered by substantially dense and tall grass. A discussion on how to address these issues are provided in the next section.

Similar to ground vegetation density, different vegetation cover types had variable impact on CWD classification accuracy. High tree and high shrub cover (HTHS) substantially decreased correctness accuracy in TLS and FLS datasets by creating many false positives. This is probably due to detailed TLS data on low-lying vegetation clumps being misclassified, which contributed to false positives. FLS data from sites with low tree and low shrub (LTLS) cover resulted in the most accurate CWD counts.

**Considerations for sensor types, data collection and processing in relation to landscape context**

We found a moderate relationship between TLS and ULS derived variables, but most of the TLS and FLS based variables were strongly correlated. High correlation between the TLS and

FLS variables is likely due to the TLS being over-represented in FLS data as TLS has higher point density, which enables it to capture more details of surface topography. As a result, the TLS data had a stronger impact on the FLS derived DSM, which consequently produced highly correlated TLS and FLS surface topographic variables. Conversely, ULS data is under-represented in FLS data and therefore the relationship between the ULS and FLS variables is weaker (Appendix 1). Future research should consider balancing the contribution from the point clouds from each sensor when fusing TLS and ULS data. The ability of the ULS sensor to collect multiple returns from above the sites allowed it to detect the ground more accurately, and as a result, it typically generated the best DSMs (Appendix 4). Conversely, the single return TLS beams did not always reach the ground as accurately as ULS data due to occlusion from dense ground vegetation and the viewing angle.

This study reported that seven TLS scans in each site could detect the majority of CWD on sites with lower or moderate ground cover; however, detection accuracy substantially decreased with increased ground cover. Based on these 7 scan, TLS data did not always capture CWD completely from all sides and experienced some occlusions due to the bigger incident angle (angle between the incoming laser pulse and surface normal) that may have prevented TLS from capturing CWD due to tall/dense vegetation blocking the laser pulse (Soudarissanane et al. 2009). Additional scans per site would improve TLS data coverage but would also require considerably more time for data collection and post-processing. Nonetheless, collecting more TLS scans per site may be necessary for sites that have high ground cover and/or increased surface variability (e.g. tall grasses or other ground objects, and/or higher topographic relief). This would decrease the incident angle of TLS scans, which would improve the accuracy of topography such as surface roughness and slope (Soudarissanane et al. 2009). Depending on the application, highly accurate surface roughness can be achieved when incident angle is $< 50^{\circ}$, which can significantly decrease the occlusion error (Milenković et al. 2015). In addition, multiple return TLS sensors would be more capable of detecting CWD through dense ground cover than the single return sensor that we used.

The ULS had a smaller incident angle and considering that the study area is an open woodland, this would have given the ULS an advantage for capturing CWD in more detail under the relatively sparse canopy. The ULS sensor that we used also records up to 5 returns per laser beam, which likely factored into performance differences between the sensors as well. The capability of ULS for detecting CWD could be further enhanced by increasing the point density per unit area. ULS sensors are now available with increased data acquisition flexibility and spatial resolution that can capture point density up to 2000 points per $m^2$, which can substantially improve the accuracy of surface topography (Levick et al. 2021). These types of sensors may be needed over more densely forested sites, where we would expect the ULS sensor to decrease in its detection accuracy due to the occlusion of the ground layer by canopy vegetation cover. The fusion of ULS and TLS data may be particularly useful in denser forests with canopy gaps where data collection from both sensors could reduce any loss of coverage. Ultimately, however, the contribution of ULS for CWD assessment would be limited by its ability to penetrate canopy vegetation. In forests with very dense canopies, it may not be possible to use ULS data for this purpose, although new sensors and platforms are being developed that may help to overcome these limitations (Hyyppä et al. 2021).

This study analyzed the XYZ coordinates of point clouds only. LiDAR provides intensity values for each collected point that could provide additional strong prediction power, which in turn may improve RF classification accuracy as grass and CWD might reflect significantly different intensity value (Charaniya et al. 2004). However, intensity data requires additional radiometric calibration (Yan et al. 2012) and validation tasks. Future research should consider incorporating information on the intensity of LiDAR returns as this can be useful for the classification of some land cover types and may improve the detection and quantification of

CWD with LiDAR data (Yan et al. 2012; Kashani et al. 2015). In addition, future research should also trial edge-preserved smoothing interpolation techniques (Al-nasrawi et al. 2017) to create DSMs, rather than TIN raster. Edge-preserving interpolation methods may decrease the surface roughness created by grasses while retaining the strong edges of CWD, and this could help mitigate errors created by false positive CWD objects from the RF model.

## Acknowledgements

We thank Paul Yeoh, Evelyn Wu, Renee Stainer, and Phoebe Hopkins for their help with data collection. This research was funded by a grant from the Australian Research Council (DE150101870) and The Australian National University Centre for Biodiversity Analysis Ignition Grant.

## Declaration of interest statement

The authors declare no conflict of interest.

## References

Al-nasrawi, M., Deng, G., and Thai, B. 2017. "Edge-aware smoothing through adaptive interpolation." *Signal, Image and Video Processing* 12 (2):347-54. doi: 10.1007/s11760-017-1164-x.

Amatulli, G., Domisch, S., Tuanmu, M. N., Parmentier, B., Ranipeta, A., Malczyk, J., and Jetz, W. 2018. "A suite of global, cross-scale topographic variables for environmental and biodiversity modeling." *Sci Data* 5:180040. doi: 10.1038/sdata.2018.40.

Belgiu, M., and Drăguţ, L. 2016. "Random forest in remote sensing: A review of applications and future directions." *ISPRS Journal of Photogrammetry and Remote Sensing* 114:24-31. doi: 10.1016/j.isprsjprs.2016.01.011.

Bergen, K. M., Goetz, S. J., Dubayah, R. O., Henebry, G. M., Hunsaker, C. T., Imhoff, M. L., Nelson, R. F., Parker, G. G., and Radeloff, V. C. 2009. "Remote sensing of vegetation 3-D structure for biodiversity and habitat: Review and implications for lidar and radar spaceborne missions." *Journal of Geophysical Research: Biogeosciences* 114 (G2). doi: 10.1029/2008jg000883.

Blanchard, S. D., Jakubowski, M. K., and Kelly, M. 2011. "Object-Based Image Analysis of Downed Logs in Disturbed Forested Landscapes Using Lidar." *Remote Sensing* 3 (11):2420-39. doi: 10.3390/rs3112420.

Boz, M. B., Calvert, K., and Brownson, J. R. 2015. "An automated model for rooftop PV systems assessment in ArcGIS using LIDAR." *AIMS Energy* 3 (3):401-20.

Breiman, L. 2001. "Random Forests." *Machine Learning* 45 (1):5-32. doi: 10.1023/A:1010933404324.

Charaniya, A. P., Manduchi, R., and Lodha, S. K. 2004. Supervised Parametric Classification of Aerial LiDAR Data. Paper presented at the 2004 Conference on Computer Vision and Pattern Recognition Workshop, 27 June-2 July 2004.

CloudCompare. 2020. Version: 2.10.2 (Zephyrus). Retrieved from http://www.cloudcompare.org/.

Conrad, O., Bechtel, B., Bock, M., Dietrich, H., Fischer, E., Gerlitz, L., Wehberg, J., Wichmann, V., and Böhner, J. 2015. "System for Automated Geoscientific Analyses (SAGA) v. 2.1.4." *Geosci. Model Dev.* 8 (7):1991-2007. doi: 10.5194/gmd-8-1991-2015.

Droppova, V. 2011. "The tools of automated generalization and building generalization in an ArcGIS environment." *Slovak Journal of Civil Engineering* 19 (1):1-7.

Duro, D. C., Franklin, S. E., and Dubé, M. G. 2012. "A comparison of pixel-based and object-based image analysis with selected machine learning algorithms for the classification of agricultural landscapes using SPOT-5 HRG imagery." *Remote Sensing of Environment* 118:259-72. doi: 10.1016/j.rse.2011.11.020.

Edwards, M. B. 2004. "Size of coarse woody debris 5 years after girdling and removal treatments in 50-year-old loblolly pine plantations." In *General Technical Reports SRS–71*, 108-13. Asheville, NC: U.S. : Department of Agriculture, Forest Service, Southern Research Station.

ESRI. 2011. ArcGIS Desktop: Release 10. Redlands. CA: Environmental Systems Research Institute.

Farnell, I., Elkin, C., Lilles, E., Roberts, A.-M., and Venter, M. 2020. "The effects of variable retention forestry on coarse woody debris dynamics and concomitant impacts on American marten habitat after 27 years." *Canadian Journal of Forest Research* 50 (9):925-35.

Friedman, J., Hastie, T., and Tibshirani, R. 2001. *The elements of statistical learning*. Vol. 1: Springer series in statistics New York.

Grizzel, J., McGowan, M., Smith, D., and Beechie, T. 2000. "Streamside buffers and large woody debris recruitment: evaluating the effectiveness of watershed analysis."

Guo, L., Chehata, N., Mallet, C., and Boukir, S. 2011. "Relevance of airborne lidar and multispectral image data for urban scene classification using Random Forests." *ISPRS Journal of Photogrammetry and Remote Sensing* 66 (1):56-66. doi: 10.1016/j.isprsjprs.2010.08.007.

Harmon, M. E., Franklin, J. F., Swanson, F. J., Sollins, P., Gregory, S. V., Lattin, J. D., Anderson, N. H., et al. 2004. "Ecology of Coarse Woody Debris in Temperate Ecosystems." In *Advances in Ecological Research*, 59-234. Academic Press.

Hijmans, R. J. 2020. raster: Geographic Data Analysis and Modeling. R package version 3.1-5. https://CRAN.R-project.org/package=raster.

Hyyppä, J., Yu, X., Hakala, T., Kaartinen, H., Kukko, A., Hyyti, H., Muhojoki, J., and Hyyppä, E. 2021. "Under-Canopy UAV Laser Scanning Providing Canopy Height and Stem Volume Accurately." *Forests* 12 (7). doi: 10.3390/f12070856.

Isenburg, M. 2012. "LAStools-efficient tools for LiDAR processing." *Available at: http: http://www.cs.unc.edu/~isenburg/lastools/*.

Kashani, A. G., Olsen, M. J., Parrish, C. E., and Wilson, N. 2015. "A Review of LIDAR Radiometric Processing: From Ad Hoc Intensity Correction to Rigorous Radiometric Calibration." *Sensors (Basel)* 15 (11):28099-128. doi: 10.3390/s151128099.

Khosravipour, A., Skidmore, A. K., Isenburg, M., Wang, T., and Hussin, Y. A. 2014. "Generating Pit-free Canopy Height Models from Airborne Lidar." *Photogrammetric Engineering & Remote Sensing* 80 (9):863-72. doi: 10.14358/pers.80.9.863.

Kuhn, M. 2020. caret: Classification and Regression Training. https://CRAN.R-project.org/package=caret.

Lefsky, M. A., Cohen, W. B., Parker, G. G., and Harding, D. J. 2002. "Lidar Remote Sensing for Ecosystem Studies." *BioScience* 52 (1):19-30. doi: 10.1641/0006-3568(2002)052[0019:lrsfes]2.0.co;2.

Levick, S. R., Whiteside, T., Loewensteiner, D. A., Rudge, M., and Bartolo, R. 2021. "Leveraging TLS as a Calibration and Validation Tool for MLS and ULS Mapping of Savanna Structure and Biomass at Landscape-Scales." *Remote Sensing* 13 (2). doi: 10.3390/rs13020257.

Lopes Queiroz, G., McDermid, G., Linke, J., Hopkinson, C., and Kariyeva, J. 2020. "Estimating Coarse Woody Debris Volume Using Image Analysis and Multispectral LiDAR." *Forests* 11 (2). doi: 10.3390/f11020141.

Lopes Queiroz, G., McDermid, G. J., Castilla, G., Linke, J., and Rahman, M. M. 2019. "Mapping Coarse Woody Debris with Random Forest Classification of Centimetric Aerial Imagery." *Forests* 10 (6). doi: 10.3390/f10060471.

Manning, A. D., Cunningham, R. B., and Lindenmayer, D. B. 2013. "Bringing forward the benefits of coarse woody debris in ecosystem recovery under different levels of grazing and vegetation density." *Biological Conservation* 157:204-14. doi: 10.1016/j.biocon.2012.06.028.

Manning, A. D., Lindenmayer, D. B., and Barry, S. C. 2004. "The conservation implications of bird reproduction in the agricultural “matrix”: a case study of the vulnerable superb parrot of south-eastern Australia." *Biological Conservation* 120 (3):363-74. doi: 10.1016/j.biocon.2004.03.008.

Manning, A. D., Lindenmayer, D. B., and Cunningham, R. B. 2007. "A study of coarse woody debris volumes in two box-gum grassy woodland reserves in the Australian Capital Territory." *Ecological Management & Restoration* 8 (3):221-4. doi: 10.1111/j.1442-8903.2007.00371.x.

Manning, A. D., Wood, J. T., Cunningham, R. B., McIntyre, S., Shorthouse, D. J., Gordon, I. J., and Lindenmayer, D. B. 2011. "Integrating research and restoration: the establishment of a long-term woodland experiment in south-eastern Australia." *Zoologist* 35 (3):633-48.

Marchi, N., Pirotti, F., and Lingua, E. 2018. "Airborne and Terrestrial Laser Scanning Data for the Assessment of Standing and Lying Deadwood: Current Situation and New Perspectives." *Remote Sensing* 10 (9). doi: 10.3390/rs10091356.

Maxwell, A. E., Warner, T. A., and Fang, F. 2018. "Implementation of machine-learning classification in remote sensing: an applied review." *International Journal of Remote Sensing* 39 (9):2784-817. doi: 10.1080/01431161.2018.1433343.

McIntyre, S., Stol, J., Harvey, J., Nicholls, A. O., Campbell, A., Reid, A., Manning, A. D., Lindenmayer, D. B., and 2010. "Biomass and floristic patterns in the ground layer vegetation of box-gum grassy eucalypt woodland in Goorooyarroo and Mulligans Flat Nature Reserves, Australian Capital Territory." *Cunninghamia: a journal of plant ecology for eastern Australia* 11 (3):319-57.

Milenković, M., Pfeifer, N., and Glira, P. 2015. "Applying Terrestrial Laser Scanning for Soil Surface Roughness Assessment." *Remote Sensing* 7:2007-45. doi: 10.3390/rs70202007.

Millard, K., and Richardson, M. 2015. "On the Importance of Training Data Sample Selection in Random Forest Image Classification: A Case Study in Peatland Ecosystem Mapping." *Remote Sensing* 7 (7):8489-515. doi: 10.3390/rs70708489.

Montealegre, A. L., Lamelas, M. T., and de la Riva, J. 2015. "A Comparison of Open-Source LiDAR Filtering Algorithms in a Mediterranean Forest Environment." *IEEE Journal of Selected Topics in Applied Earth Observations and Remote Sensing* 8 (8):4072-85. doi: 10.1109/jstars.2015.2436974.

Mücke, W., Hollaus, M., Pfeifer, N., Schroiff, A., and Deák, B. 2013. "Comparison of discrete and full-waveform ALS for dead wood detection." *ISPRS Annals of Photogrammetry, Remote Sensing and Spatial Information Sciences* II-5/W2:199-204. doi: 10.5194/isprsannals-II-5-W2-199-2013.

Pasher, J., and King, D. J. 2009. "Mapping dead wood distribution in a temperate hardwood forest using high resolution airborne imagery." *Forest Ecology and Management* 258 (7):1536-48. doi: 10.1016/j.foreco.2009.07.009.

Pesonen, A., Leino, O., Maltamo, M., and Kangas, A. 2009. "Comparison of field sampling methods for assessing coarse woody debris and use of airborne laser scanning as auxiliary information." *Forest Ecology and Management* 257 (6):1532-41. doi: 10.1016/j.foreco.2009.01.009.

Polewski, P., Yao, W., Heurich, M., Krzystek, P., and Stilla, U. 2017. "A voting-based statistical cylinder detection framework applied to fallen tree mapping in terrestrial laser scanning point clouds." *ISPRS Journal of Photogrammetry and Remote Sensing* 129:118-30. doi: 10.1016/j.isprsjprs.2017.04.023.

Probst, P., and Boulesteix, A.-L. 2017. "To tune or not to tune the number of trees in random forest." *J. Mach. Learn. Res.* 18 (1):6673–90.

QGIS.org. 2021. QGIS Geographic Information System. QGIS Association. http://www.qgis.org.

R Core Team. 2020. R: A Language and Environment for Statistical Computing. . Vienna, Austria. R Foundation for Statistical Computing. https://www.R-project.org/.

Richardson, J., and Moskal, L. 2016. "An Integrated Approach for Monitoring Contemporary and Recruitable Large Woody Debris." *Remote Sensing* 8 (9). doi: 10.3390/rs8090778.

Šašak, J., Gallay, M., Kaňuk, J., Hofierka, J., and Minár, J. 2019. "Combined Use of Terrestrial Laser Scanning and UAV Photogrammetry in Mapping Alpine Terrain." *Remote Sensing* 11 (18):2154.

Shokirov, S. 2021. "Using multi-platform LiDAR to assess vegetation structure for woodland forest fauna " PhD thesis, Australian National University. doi: 10.25911/ZYAV-6R15.

Shokirov, S., Levick, S. R., Jucker, T., Yeoh, P., and Youngentob, K. 2020. "Comparison of TLS and ULS Data for Wildlife Habitat Assessments in Temperate Woodlands." In *IGARSS 2020 - 2020 IEEE International Geoscience and Remote Sensing Symposium*, 6097-100.

Smikrud, K. M., and Prakash, A. 2013. "Monitoring Large Woody Debris Dynamics in the Unuk River, Alaska Using Digital Aerial Photography." *GIScience & Remote Sensing* 43 (2):142-54. doi: 10.2747/1548-1603.43.2.142.

Soudarissanane, S., Lindenbergh, R., Menenti, M., and Teunissen, P. 2009. "Incidence angle influence on the quality of terrestrial laser scanning points." *Proceedings ISPRS Workshop Laserscanning 2009, 1-2 Sept 2009, Paris, France* 38.

Stereńczak, K., Ciesielski, M., Balazy, R., and Zawiła-Niedźwiecki, T. 2016. "Comparison of various algorithms for DTM interpolation from LIDAR data in dense mountain forests." *European Journal of Remote Sensing* 49 (1):599-621. doi: 10.5721/EuJRS20164932.

SZ DJI TECHNOLOGY CO., L. 2018. "DJI GS Pro User Manual." In.

Vandekerkhove, K., De Keersmaeker, L., Menke, N., Meyer, P., and Verschelde, P. 2009. "When nature takes over from man: Dead wood accumulation in previously managed oak and beech woodlands in North-western and Central Europe." *Forest Ecology and Management* 258 (4):425-35. doi: 10.1016/j.foreco.2009.01.055.

West, P. W., Cawsey, E. M., Stol, J., and Freudenberger, D. 2008. "Firewood harvest from forests of the Murray-Darling Basin, Australia. Part 1: Long-term, sustainable supply available from native forests." *Biomass and Bioenergy* 32 (12):1206-19. doi: https://doi.org/10.1016/j.biombioe.2008.02.017.

Windrim, L., Bryson, M., McLean, M., Randle, J., and Stone, C. 2019. "Automated Mapping of Woody Debris over Harvested Forest Plantations Using UAVs, High-Resolution Imagery, and Machine Learning." *Remote Sensing* 11 (6). doi: 10.3390/rs11060733.

Woldendorp, G., and Keenan, R. J. 2005. "Coarse woody debris in Australian forest ecosystems: A review." *Austral Ecology* 30 (8):834-43. doi: 10.1111/j.1442-9993.2005.01526.x.

Yan, W. Y., Shaker, A., Habib, A., and Kersting, A. P. 2012. "Improving classification accuracy of airborne LiDAR intensity data by geometric calibration and radiometric correction." *ISPRS Journal of Photogrammetry and Remote Sensing* 67:35-44. doi: https://doi.org/10.1016/j.isprsjprs.2011.10.005.

Yrttimaa, T., Saarinen, N., Luoma, V., Tanhuanpää, T., Kankare, V., Liang, X., Hyyppä, J., Holopainen, M., and Vastaranta, M. 2019. "Detecting and characterizing downed dead wood using terrestrial laser scanning." *ISPRS Journal of Photogrammetry and Remote Sensing* 151:76-90. doi: 10.1016/j.isprsjprs.2019.03.007.

## Tables

Table 1. Descriptions of topographic variables.

| Variable name | Description |
|---|---|
| Digital surface model (DSM) | 0.1 m grid calculated from normalized points below 1.3 m using TIN interpolation method (Isenburg 2012). |
| Roughness | Roughness is calculated as the largest inter-cell difference of a focal cell and its 8 neighboring pixels (Amatulli et al. 2018) |
| Slope | Slope expresses the degree of elevation change in the direction of the steepest descent (Amatulli et al. 2018). |
| Aspect | Aspect is the orientation of slope. It is measured clockwise in degrees from 0 to 360, where 0 is north-facing, 90 is east-facing, 180 is south-facing, and 270 is west-facing (Amatulli et al. 2018). |
| Topographic ruggedness index (TRI) | TRI is the average of the absolute differences in elevation between a focal cell and its neighboring cells. Zero values correspond to flat surfaces whereas positive values correspond to mountain areas (Amatulli et al. 2018) |
| Topographic position index (TPI) | TPI compares the elevation of a focal cell and the mean of its 8 neighboring cells. Positive values represent ridges, negative values correspond to valleys and zero values correspond to flat areas (Amatulli et al. 2018). |

Table 2. Random forest (RF) classification accuracy. Confusion matrices describe comparison between the predicted classes of pixels by RF model and independent testing data. Both predicted and testing dataset represent the number of pixels. a) Terrestrial laser scanner (TLS), b) an unoccupied aerial vehicle laser scanner (ULS), c) fused TLS and ULS (FLS) data.

a)

| | | **Hold-out testing data** | | | |
|---|---|---|---|---|---|
| **Predicted data** | | CWD | Shrub | Grass | **User's accuracy** |
| | CWD | 6592 | 2574 | 541 | 67.9% |
| | Shrub | 2946 | 6559 | 295 | 66.9% |
| | Grass | 616 | 425 | 6346 | 85.9% |
| | **Producer's accuracy** | 64.9% | 68.6% | 88.4% | |
| | **Overall accuracy** | 72.5% | | | |

b)

| | | **Hold-out testing data** | | | |
|---|---|---|---|---|---|
| **Predicted data** | | CWD | Shrub | Grass | **User's accuracy** |
| | CWD | 21941 | 5257 | 2968 | 72.7% |
| | Shrub | 3194 | 8128 | 100 | 71.2% |
| | Grass | 3744 | 859 | 19509 | 80.9% |
| | **Producer's accuracy** | 76.0% | 57.1% | 86.4% | |
| | **Overall accuracy** | 75.5% | | | |

c)

| | | **Hold-out testing data** | | | |
|---|---|---|---|---|---|
| **Predicted data** | | CWD | Shrub | Grass | **User's accuracy** |
| | CWD | 15243 | 3974 | 2792 | 69.3% |
| | Shrub | 2947 | 13969 | 497 | 80.2% |
| | Grass | 3760 | 3185 | 32397 | 82.3% |
| | **Producer's accuracy** | 69.4% | 66.1% | 90.8% | |
| | **Overall accuracy** | 78.2% | | | |

Table 3. Overall completeness and correctness of coarse woody debris (CWD) counts in eighteen independent validation sites using data from a terrestrial laser scanner (TLS), an unoccupied aerial vehicle laser scanner (ULS), fused TLS and ULS data (FLS). Sites included four vegetation types (1) high tree, high shrub cover (HTHS), 2) high tree, low shrub cover (HTLS), 3) low tree, low shrub cover (LTLS), and 4) low tree, high shrub cover (LTHS)) and three ground vegetation densities (high, medium, low).

| Site | Veg class | CWD type | Ground veg. type | TLS | | ULS | | FLS | |
|---|---|---|---|---|---|---|---|---|---|
| | | | | Complete-ness | Correct-ness | Complete-ness | Correct-ness | Complete-ness | Correct-ness |
| MF11A-4 | LTHS | clumped | High | 66.7 | 43.1 | 60.6 | 60.6 | 66.7 | 41.5 |
| MF11A-2 | LTHS | combined | Medium | 66.2 | 41.0 | 46.2 | 81.1 | 64.6 | 50.6 |
| MF11A-3 | LTHS | dispersed | Medium | 60.6 | 40.0 | 40.6 | 39.4 | 60.6 | 48.8 |
| MF27A-2 | LTHS | dispersed | Low | 71.4 | 73.5 | 64.7 | 40.7 | 82.9 | 76.3 |
| MF22A-2 | HTHS | clumped | High | 63.2 | 22.6 | 65.8 | 46.3 | 60.5 | 24.5 |
| MF22A-3 | HTHS | dispersed | High | 48.7 | 11.9 | 56.4 | 47.8 | 56.4 | 27.2 |
| MF22A-4 | HTHS | combined | High | 64.4 | 25.4 | 82.2 | 41.1 | 46.7 | 20.8 |
| MF34-1 | HTLS | clumped | Low | 46.6 | 87.2 | 55.4 | 62.1 | 72.6 | 75.7 |
| MF34-4 | HTLS | combined | Medium | 50.5 | 30.9 | 61.5 | 64.1 | 54.8 | 49.0 |
| MF34-3 | HTLS | dispersed | Low | 61.3 | 70.8 | 60.5 | 75.4 | 48.6 | 58.1 |
| WG150A-3 | HTLS | clumped | Low | 69.6 | 44.4 | 56.5 | 33.3 | 76.1 | 47.3 |
| WG150A-2 | HTLS | dispersed | Low | 62.7 | 30.8 | 58.8 | 29.4 | 62.7 | 53.3 |
| WG63A-1 | LTLS | combined | Medium | 75.0 | 94.7 | 72.2 | 71.2 | 86.1 | 72.1 |
| WG63A-4 | LTLS | combined | Low | 69.9 | 96.2 | 56.8 | 64.6 | 71.6 | 84.1 |
| WG148-3 | LTLS | combined | Medium | 38.0 | 85.7 | 58.8 | 58.0 | 75.9 | 81.1 |
| WG148-4 | LTLS | dispersed | Medium | 55.8 | 78.4 | 39.6 | 30.0 | 69.2 | 65.5 |
| WG148-2 | LTLS | clumped | Medium | 19.6 | 30.3 | 66.0 | 33.3 | 68.6 | 60.3 |
| WG92-3 | LTLS | clumped | Low | 35.1 | 92.9 | 37.8 | 51.9 | 81.1 | 65.2 |
| | | | **Max** | **75.0** | **96.2** | **82.2** | **81.1** | **86.1** | **84.1** |
| | | | **Min** | **19.6** | **11.9** | **37.8** | **29.4** | **46.7** | **20.8** |
| | | | **Mean** | **57.0** | **55.6** | **57.8** | **51.7** | **67.0** | **55.6** |
| | | | **Median** | **62.0** | **43.8** | **58.8** | **49.8** | **67.6** | **55.7** |

Table 4. Coarse woody debris (CWD) count accuracy by low, medium and high density ground vegetation sites using data from a terrestrial laser scanner (TLS), an unoccupied aerial vehicle laser scanner (ULS), and fused TLS and ULS data (FLS).

| Ground vegetation density | TLS | | ULS | | FLS | |
|---|---|---|---|---|---|---|
| | Completeness | Correctness | Completeness | Correctness | Completeness | Correctness |
| Low | 59.5 | 70.8 | 55.8 | 51.1 | 70.8 | 65.7 |
| Medium | 52.2 | 57.3 | 55.0 | 53.9 | 68.6 | 61.1 |
| High | 60.7 | 25.8 | 66.3 | 49.0 | 57.6 | 28.5 |

Table 5. Coarse woody debris (CWD) count accuracy by four vegetation types: low tree high shrub (LTHS), high tree high shrub (HTHS), high tree low shrub (HTLS), and low tree low shrub (LTLS) using data from a terrestrial laser scanner (TLS), an unoccupied aerial vehicle laser scanner (ULS), and fused TLS and ULS data (FLS).

| Vegetation types | TLS | | ULS | | FLS | |
|---|---|---|---|---|---|---|
| | Completeness | Correctness | Completeness | Correctness | Completeness | Correctness |
| LTHS | 66.2 | 49.4 | 53.0 | 55.5 | 68.7 | 54.3 |
| HTHS | 58.8 | 20.0 | 68.1 | 45.1 | 54.5 | 24.1 |
| HTLS | 58.2 | 52.8 | 58.5 | 52.9 | 63.0 | 56.7 |
| LTLS | 48.9 | 79.7 | 55.2 | 51.5 | 75.4 | 71.4 |

## Figures

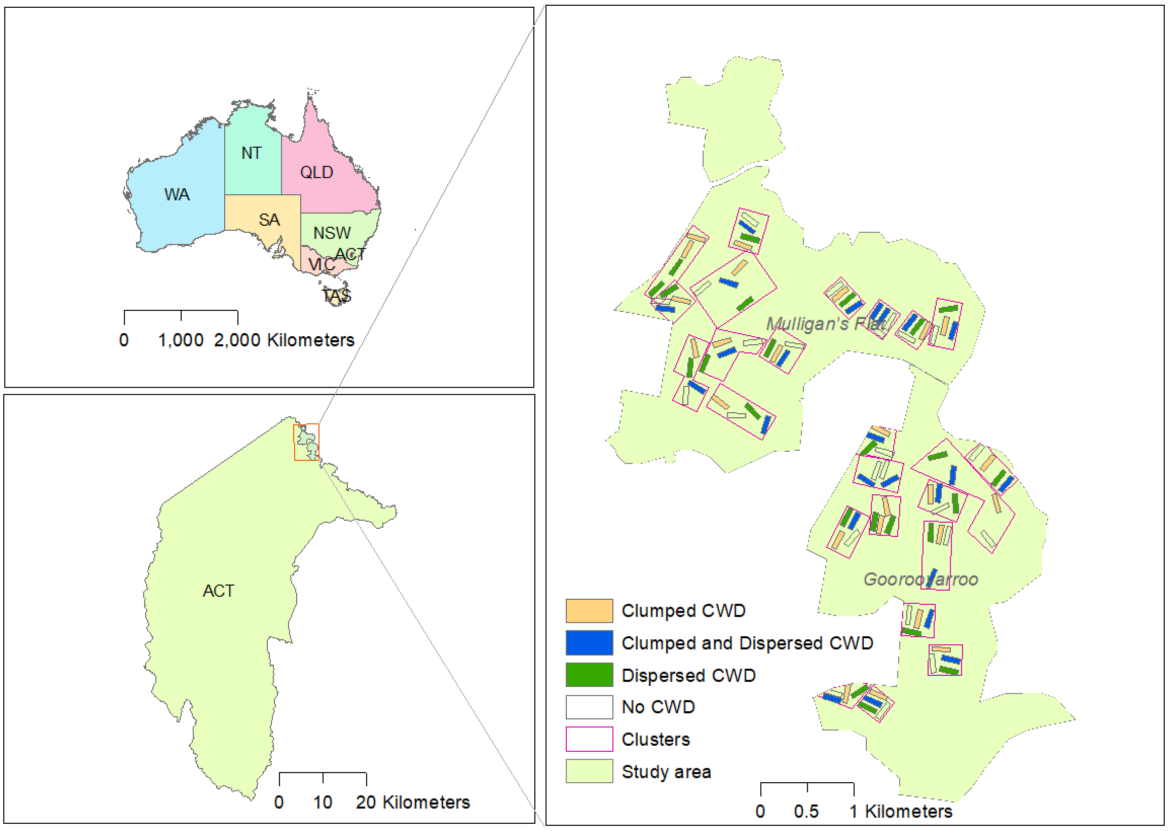


Figure 1. Map of the study area in Australia (top left) and inset of the Australian Capital Territory (bottom left) showing the location of Mulligan's Flat and Goorooyarroo Nature Reserves (right) with experimental restoration plots containing different treatments of coarse woody debris (CWD).


Figure 2. Images of dispersed (*a*) and clumped (*b*, *c*) coarse woody debris in low (*a*), medium (*c*), and high (*b*) ground vegetation cover categories.

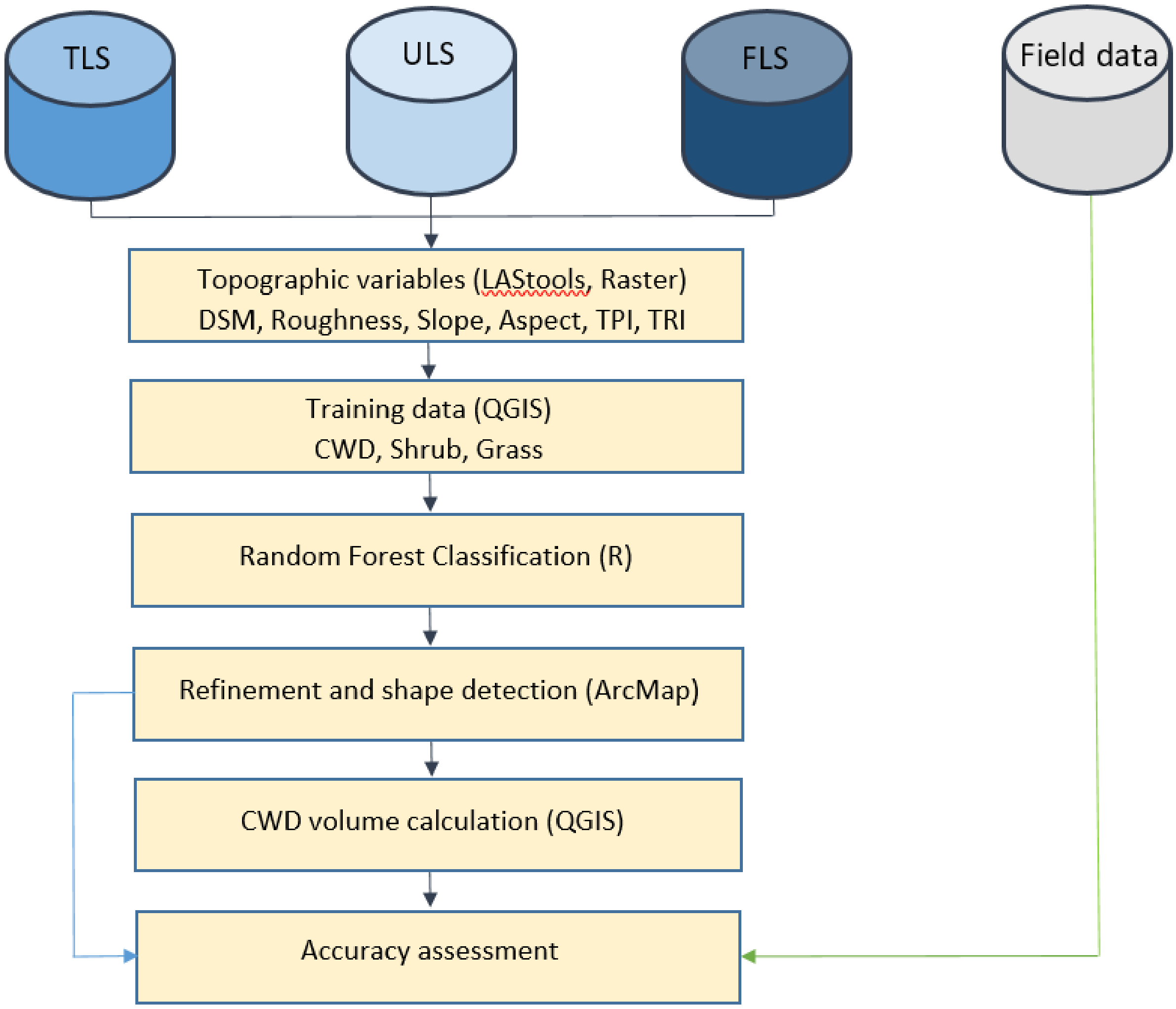


Figure 3. Workflow of the coarse woody debris (CWD) extraction method, including software and packages used. TLS is Terrestrial laser scanner, ULS is unoccupied aerial vehicle laser scanner and FLS is fused ULS and TLS data.

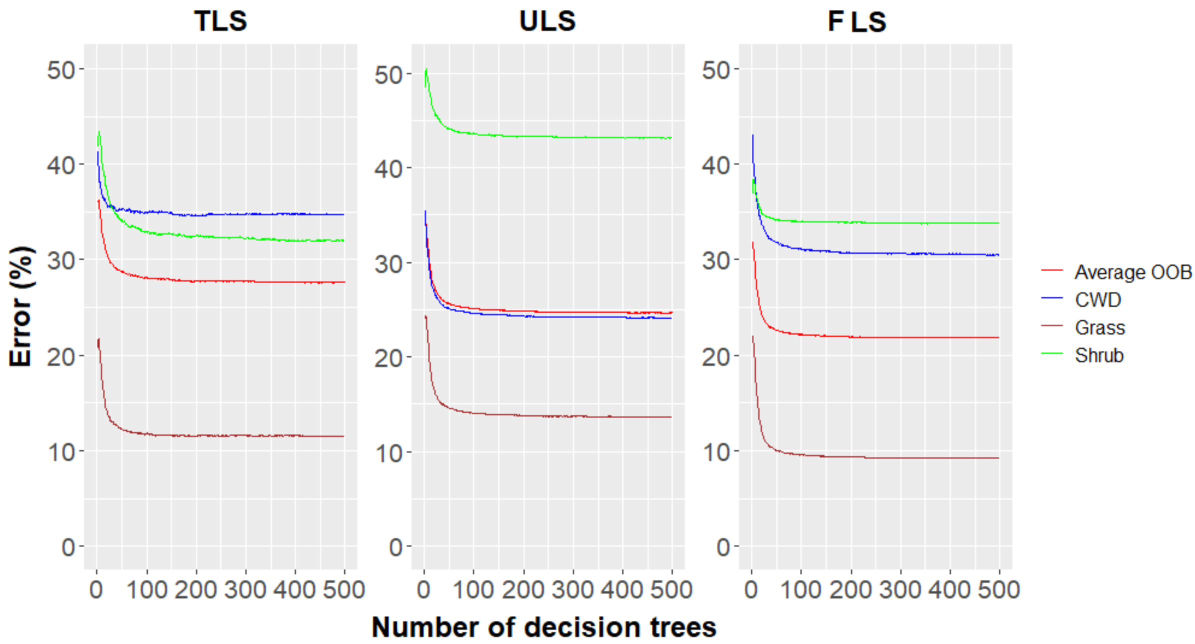


Figure 4. Random forest accuracy assessment of terrestrial laser scanner (TLS), an unoccupied aerial vehicle laser scanner (ULS), fused TLS and ULS (FLS) data for classifying coarse woody debris (CWD), grass and shrubs with out-of-bag (OOB) error. OOB is calculated by comparing classified training data with excluded (out-of-bag) training data.

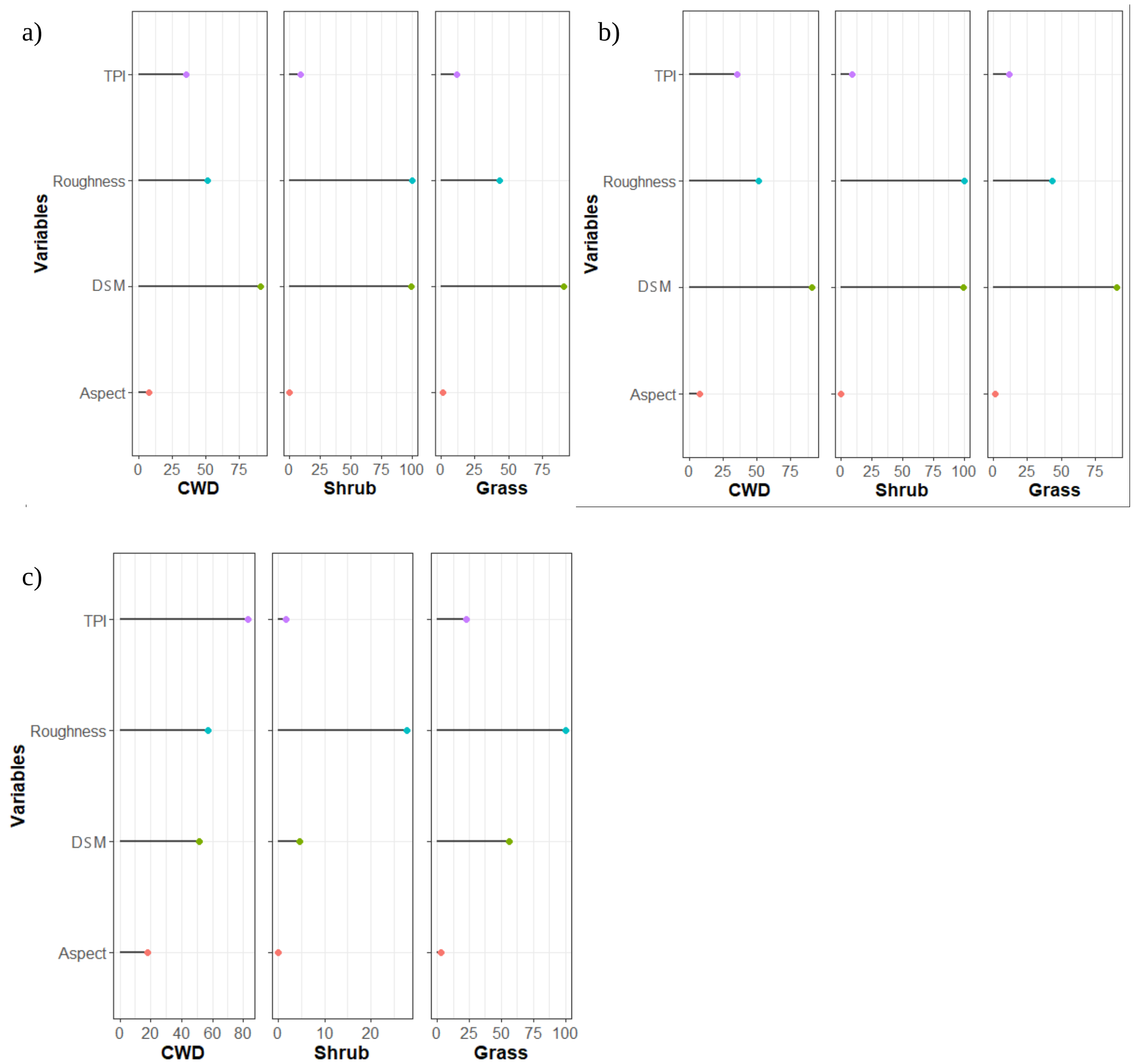


Figure 5. Predictor variable importance for random forest classification of three landscape features (coarse woody debris (CWD), shrub and grass) with LiDAR data from (a) terrestrial laser scanner (TLS), (b) an unoccupied aerial vehicle laser scanner (ULS) and (c) fused TLS and ULS data (FLS). Abbreviations stand for digital surface model (DSM), topographic position index (TPI), topographic ruggedness index (TRI).

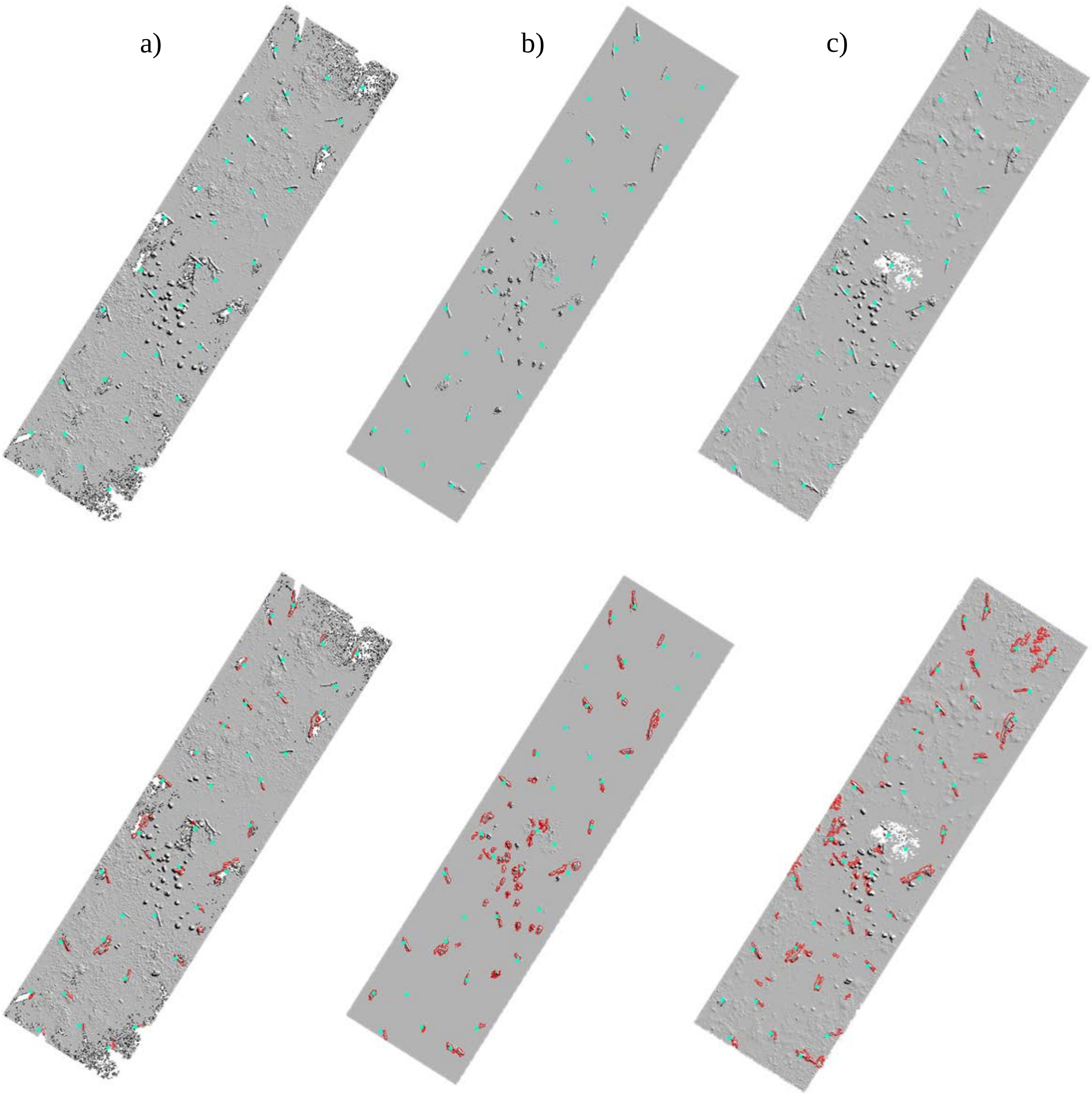


Figure 6. Shaded relief (top) and mapped coarse woody debris (CWD) (bottom) images of one sample site with combined CWD (dispersed and clumped). Cyan dots indicate locations of CWD measured in the field, red polygons represent classified CWD. Images are from (a) terrestrial laser scanner (TLS), (b) an unoccupied aerial vehicle laser scanner (ULS) and (c) fused TLS and ULS data (FLS).

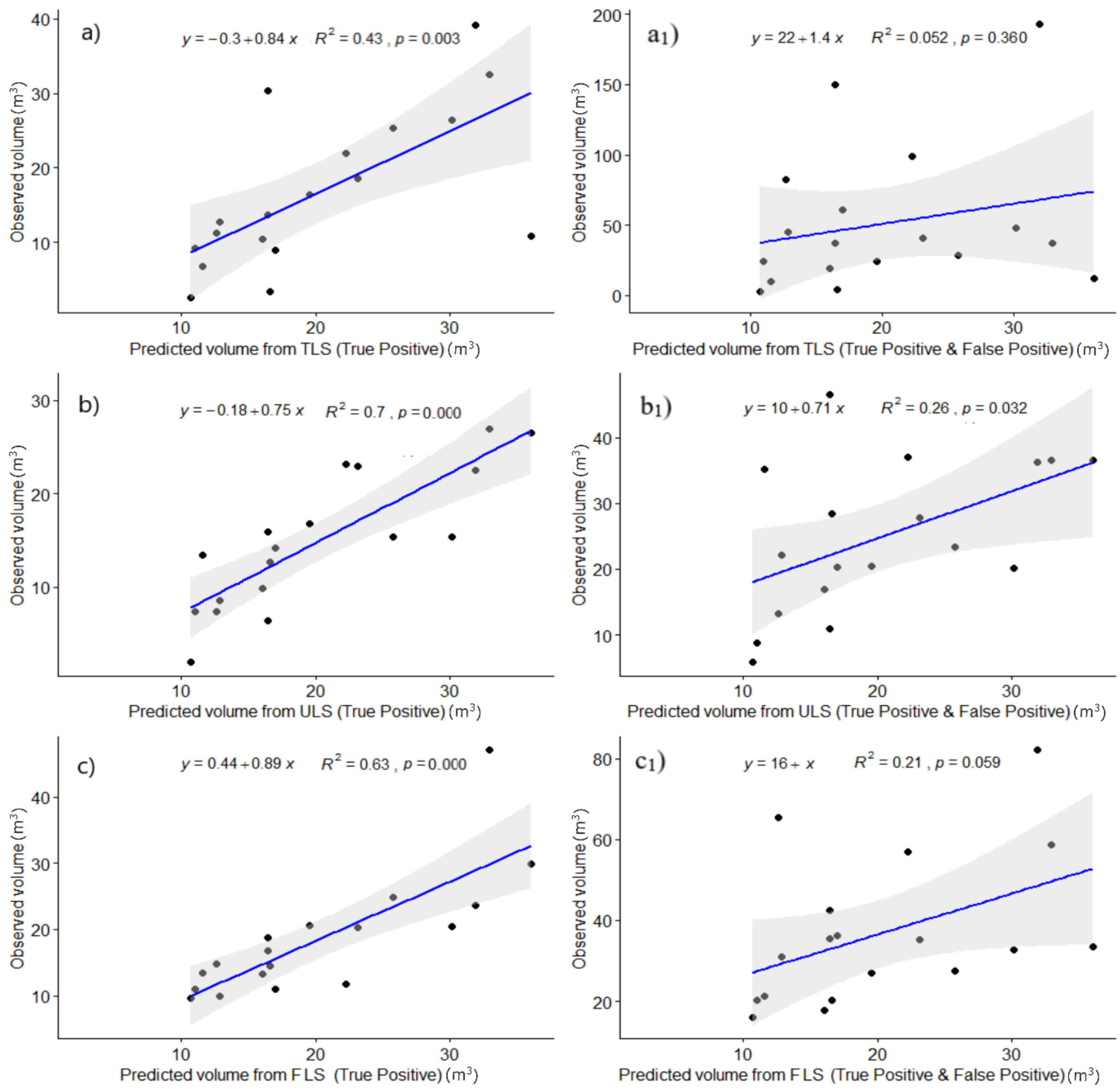


Figure 7. Relationship between observed and detected coarse woody debris (CWD) volume across the three data types; (a, $a_1$) terrestrial laser scanner (TLS), (b, $b_1$) an unoccupied aerial vehicle laser scanner (ULS), (c, $c_1$) fused TLS and ULS data (FLS). True positives only are shown in a, b, and c. True and false positives are shown in $a_1$, $b_1$, and $c_1$.

## Appendices

Appendix 1. Pearson's correlation indexes between the surface topographic variables derived from the (a) Terrestrial laser scanner (TLS) and an unoccupied aerial vehicle laser scanner (ULS), (b) a TLS and FLS (i.e., fused ULS and TLS data), (c) ULS and FLS data. Digital surface model (DSM), topographic position index (TPI), topographic ruggedness index (TRI).

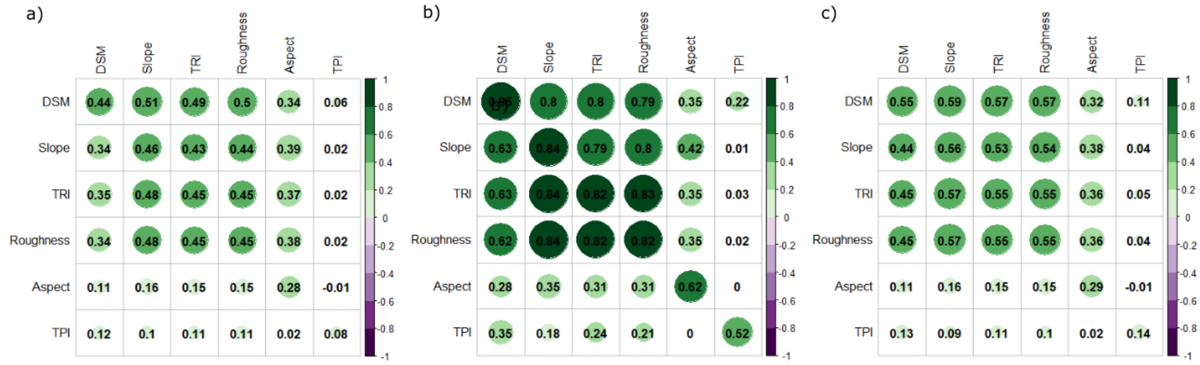

Appendix 2. Boxplots show the distribution of measured coarse woody debris (CWD) data. Upper, mid and lower horizontal lines of the box indicate 1$^{th}$, median and 3$^{rd}$ quartiles. Red dots inside a boxplot are mean values. Whiskers extend to the highest and lowest extreme of observations, and the dots on the whiskers are outliers.

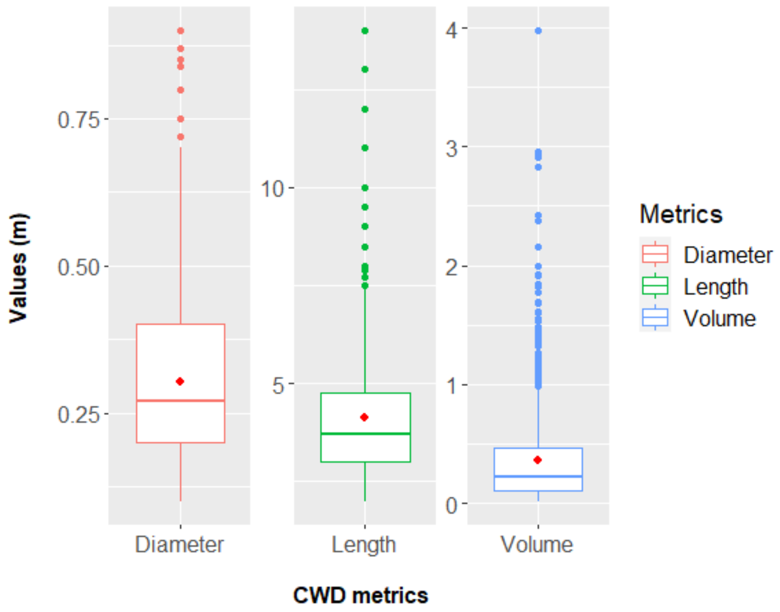

Appendix 3. Pearson's pairwise correlations between the variables calculated from (a) terrestrial laser scanner (TLS), (b) an unoccupied aerial vehicle laser scanner (ULS) and (c) fused TLS and ULS data (FLS). Abbreviations stand for Digital surface model (DSM), topographic position index (TPI), and topographic ruggedness index (TRI).

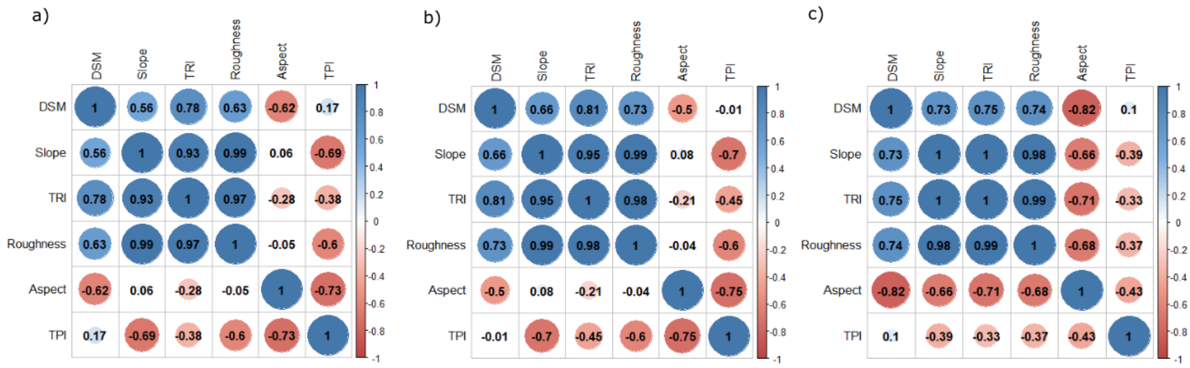

Appendix 4.

The digital surface model (DSM) samples from the (a) terrestrial laser scanner (TLS), (b) unoccupied aerial vehicle laser scanner (ULS), (c) a fusion of TLS and ULS data (FLS).